journal

J. Am. Ceram. Soc., **99** [4] 1412–1419 (2016)
DOI: 10.1111/jace.14120

$MoSi_2$ Oxidation in 670–1498 K Water Vapor

Elizabeth Sooby Wood,[‡,†] Stephen S. Parker,[‡,§] Andrew T. Nelson,[‡] and and Stuart A. Maloy[‡]

[‡]Materials Science and Technology Division, Los Alamos National Laboratory, Los Alamos, New Mexico

[§]Department of Nuclear Engineering, University of California, Berkeley, Berkeley, California

Molybdenum disilicide ($MoSi_2$) has well documented oxidation resistance at high temperature (T > 1273 K) in dry O_2 containing atmospheres due to the formation of a passive SiO_2 surface layer. However, its behavior under atmospheres where water vapor is the dominant species has received far less attention. Oxidation testing of $MoSi_2$ was performed at temperatures ranging from 670–1498 K in both 75% water vapor and synthetic air (Ar-O_2, 80%–20%) containing atmospheres. Here the thermogravimetric and microscopy data describing these phenomena are presented. Over the temperature range investigated, $MoSi_2$ displays more mass gain in water vapor than in air. The oxidation kinetics observed in water vapor differ from that of the air samples. Two volatile oxides, $MoO_2(OH)_2$ and $Si(OH)_4$, are thought to be the species responsible for the varied kinetics, at 670–877 K and at 1498 K, respectively. Increased oxidation (140–300 mg/cm^2) was observed from 980–1084 K in water vapor, where passivation is observed in air.

I. Introduction

Molybdenum disilicide ($MoSi_2$) has been proposed as a high temperature, corrosion-resistant material since its discovery in 1907.[1] It was first used for high-temperature furnace elements in 1953 and since the 1990s used as a protective coating for high-temperature industrial applications, such as turbine airfoils, combustion chambers, and missile nozzles.[2] The oxidation behavior of $MoSi_2$ and $MoSi_2$ composites have been extensively studied in O_2 containing atmospheres up to 1973 K. However, its oxidation behavior in water vapor is largely unknown. This behavior must be understood if $MoSi_2$ is to be considered for use in oxidizing atmospheres where water vapor rather than oxygen is the primary oxidizing reactant.

(1) $MoSi_2$ Oxidation in Dry Atmospheres

$MoSi_2$ displays "pesting" when subjected to air oxidation experiments.[3–5] The temperature range for pest formation is reported at temperatures varying from 623–873 K. Full disintegration of $MoSi_2$ has been observed in O_2 containing environments after long duration (100 h) exposures in this temperature range.[3,5] Above 873 K, $MoSi_2$ begins to display excellent oxidation resistance, due to the formation of a passivating SiO_2 layer. The primary $MoSi_2$ oxidation reactions in dry O_2 atmospheres are as follows:

$$2MoSi_2 + 7O_2(g) \rightarrow 2MoO_3 + 4SiO_2 \quad (1)$$

$$5MoSi_2 + 7O_2(g) \rightarrow Mo_5Si_3 + 7SiO_2 \quad (2)$$

The temperature regime where pesting is a concern is dictated by the behavior of MoO_3 when formed according to Eq. (1) above.[6] MoO_3 behavior dominates the response of Mo oxidation in air and water vapor, as recently shown by Nelson and Sooby *et al.*[7] At temperatures below roughly 873 K, MoO_3 will remain a solid and form whiskers throughout the material. This causes expansion of the bulk material and exposure of unoxidized $MoSi_2$, preventing the SiO_2 from forming a protective layer.[8] Above 873 K, the MoO_3 vapor pressure begins to play a significant role in the oxidation. As the MoO_3 is volatilized, the SiO_2 is capable of forming a continuous protective layer, inhibiting further oxidation. It is reported that Mo_5Si_3 forms at the Si depleted interface between the bulk $MoSi_2$ and SiO_2 due to the rapid diffusion of Si as displayed in Eq. (2).[6]

Figure 1 displays an Ellingham-type diagram for several possible reactions of $MoSi_2$ and its resulting oxides in both air and H_2O containing atmospheres. It is noted that the most energetic of these reactions in air containing atmospheres are described in Eqs. 1 and 2 with the addition of the reaction described in Eq. (3)

$$MoSi_2 + 3O_2(g) \rightarrow MoO_2 + 2SiO_2 \quad (3)$$

However, MoO_2 will readily oxidize to MoO_3 in O_2 containing atmospheres. Therefore, MoO_3 is the resulting final oxide in air exposures, until it becomes volatile.

(2) $MoSi_2$ Oxidation in Water Vapor Containing Atmospheres

The data available for water vapor containing atmospheres are limited to a small range of temperatures. Hansson *et al.* found that the oxidation rate of a $MoSi_2$-composite increased with the addition of 10% water vapor to an O_2 containing atmosphere, with the peak rate reported at 743, 40 K lower than the peak oxidation temperature in pure O_2.[4] In addition, the study reports increased mass loss at higher temperatures with the addition of 10% water vapor. Referring to Fig. 1 in the presence of both O_2 and H_2O a very energetic reaction can occur resulting in the volatile Mo hydroxide species $MoO_2(OH)_2$.

$$3.5O_2(g) + MoSi_2 + H_2O(g) \rightarrow MoO_2(OH)_2 + 2SiO_2 \quad (4)$$

However, exposure to Ar, Ar + 10% water vapor, and Ar + 40% water vapor at 723 K resulted in reportedly negligible mass gain.[4] Looking to Fig. 1, the reactions between $MoSi_2$ and steam leading to volatiles are much less energetic. The effect of water vapor on $MoSi_2$ oxidation was subsequently explored to 973 K in an O_2 + 10% water vapor atmosphere.[9] Increased mass loss, in agreement with Hansson *et al.*, indicated an increase in oxidation with the addition of water vapor to O_2 containing environments. No other studies focused on the oxidation of $MoSi_2$ in water vapor have been conducted to the authors' knowledge.

D. Butt—contributing editor

Manuscript No. 37399. Received August 24, 2015; approved December 11, 2015.
[†]Author to whom correspondence should be addressed. e-mail: sooby@lanl.gov

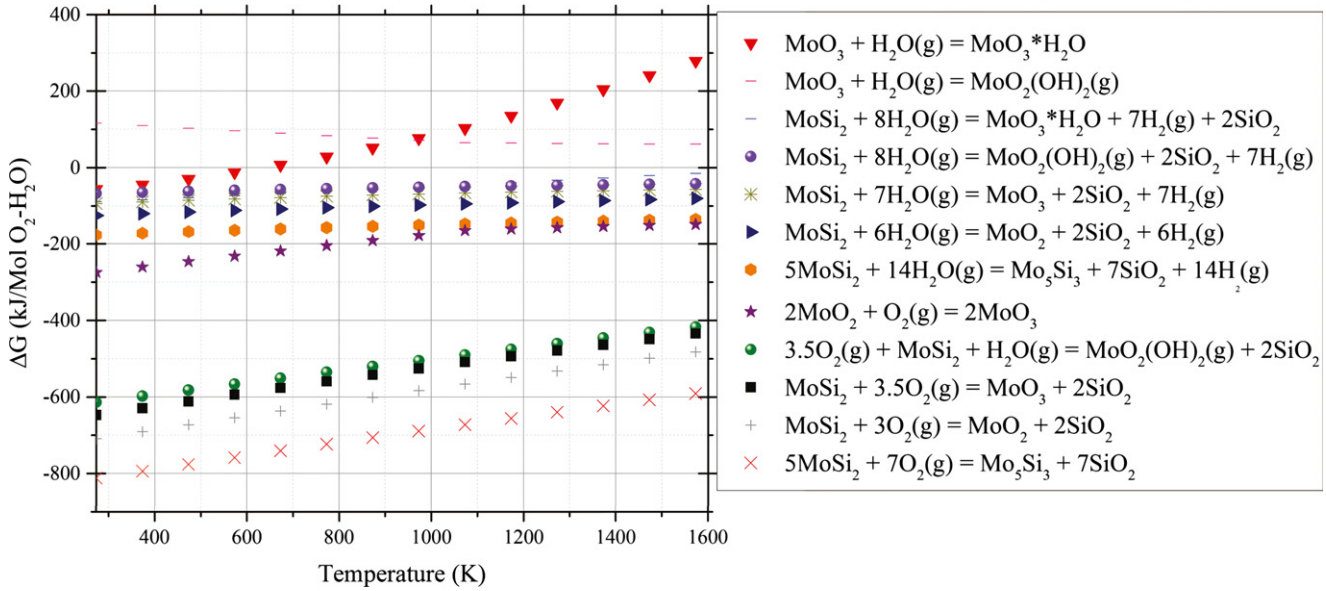

Fig. 1. Ellingham-type diagram plotting the change in the Gibbs Free Energy of a number of relevant oxidation reactions in both O_2 and H_2O containing atmospheres. Data obtained using HSC Chemistry 7 Software.

II. Experimental Method

$MoSi_2$ obtained from Goodfellow was segmented into 0.07 cm^3 parallelepipeds and then ground and polished using SiC paper to 1200 grit (U.S.) on all six sides. The prepared samples measured to be 80% theoretical $MoSi_2$ density (6.26 g/cm^3). The anticipated effect of decreased density on the oxidation behavior observed is elaborated upon in the Discussion section of this article. The resulting samples were cleaned using acetone, rinsed with methanol, and allowed to dry. The mass of each sample was measured using a balance (XP205, Mettler-Toledo, Columbus, Ohio) calibrated to 0.1 mg. To calculate the total surface area of each block, the length and width of each sample side were measured to a 0.1 mm accuracy, using digital calibers.

A simultaneous thermal analyzer (STA 449 F3, Netzsch Instruments, Selb, Germany) equipped with a water vapor furnace and water vapor generator (DV2ML, Astream, Germany) was used to measure the mass change as a function of both temperature and time. A thermocouple calibration was performed using Ni, Au, Ag, Al, and Zn melt point standards (6.223.5-91.3, Netzsch). The isothermal temperatures were corrected to reflect this calibration factor. The sample was placed on an Al_2O_3 platform in the STA. The furnace tube, sample holder, and all internal fixturing were Al_2O_3. The sample chamber was evacuated and backfilled three times to minimize the effect of residual oxygen on the oxidation behavior of the samples. In-line oxygen sensors (RapidOx OEM447; Cambridge Sensotec, Saint Ives, UK) were used to monitor the oxygen content in both the gas being delivered to the system and the exhaust gas leaving the system.

Two oxidizing atmospheres were used in this study. Synthetic air produced by mixing ultra-high purity Ar and pure O_2 (Ar–O_2, 80%–20%) was used to compare against literature data for $MoSi_2$ oxidation at temperatures ranging from 670–1498 K. Water vapor exposures were performed from 670–1498 K at approximately 100 K increments. The sample was ramped to the isothermal test temperature in Ar at 10 K/min. Negligible mass gain was observed during the ramp to the isotherm (<0.1% mass change). The sample was held at the test temperature for 15 min to allow the system to stabilize under flowing Ar before water vapor was introduced into the system. The oxygen content of the exhaust was less than 10 parts per million (ppm) O_2 for all experiments, ensuring that water vapor was the dominant oxidizing species for all testing. The water vapor generator supplied 5.26 g/h to the STA. Ar was used as a carrier gas to limit balance fluctuations while steam flowed into the system. The transfer lines used to deliver the steam to the STA were held at 473 K. In addition, 20 mL/min Ar was purged through the balance as a protective gas. It was calculated that the sample was exposed to 0.55 ATM water vapor during testing. The steam was turned off at the end of the isotherm, and the system cooled at 20 K/min under Ar.

Samples were analyzed by scanning electron microscopy (SEM). Two orientations were observed. The as-oxidized surface of each sample was imaged initially to analyze the microstructure of the oxide formed during exposure. For these as-oxidized surface samples, no surface preparation was performed in order to preserve the surface oxide. Samples were coated with Au prior to analysis using a sputter coater. The samples were also cross-sectioned, potted in epoxy, polished to 0.25 μm diamond suspension and coated to image the cross-section of the oxidized sample. The first form of imaging allowed for visualization of the microstructure of the as-formed oxide, while the second provided observations of the depth of oxidation into the bulk of the sample. Elemental analysis was performed by energy dispersive spectroscopy (EDS) using a combination of spot and line scans over the cross-sectioned samples. Both the oxidation interface (edge of the cross-sectioned samples) and the bulk of the samples were analyzed. X-ray diffraction was performed on the sample surface to identify the oxide phases that formed during both air and water vapor exposure, using a Bruker XRD (D2 Phaser; Bruker AXS, Madison, WI). A two theta range of 10°–90°, 0.01° step size and 1 s dwell time were used for all, but two samples. For the 1395 and 1498 K water vapor samples, a 5 s dwell time was used to increase the signal-to-noise ratio of the scan.

III. Results

Table I provides a summary of results for $MoSi_2$ exposed to water vapor.

(1) Thermogravimetric Analysis Results

Figure 2 displays the $MoSi_2$ mass gain normalized to surface area (mg/cm^2) for each 100 K test increasing from 670–1498 K in water vapor. Four different oxidation kinetic regimes are identified in the preliminary water vapor testing.

Table I. Summary of Results for H_2O Isothermal Oxidation Testing of $MoSi_2$

H_2O Exposure temperature (K)	Isothermal dwell time (h)	Total mass gain (mg/cm^2)	Parobolic oxidation rate constant [mg/(cm^2-h$^{(1/2)}$)]	Comments on kinetics	Phases identified following exposure XRD and EDS Analysis
670	24	3.03	0.598	Parobolic	$MoSi_2$
773	20	3.9	0.91	Parobolic	$MoSi_2$
877	20	18.95	N/A	Nonpassivating, nonlinear oxidation	†
980	20	298.21	N/A	nonpassIvating, nonlinear, rapid oxidation	$MoSi_2$, MoO_2
1084	20	141.62	N/A	Nonpassivating, nonlinear, rapid oxidation	$MoSi_2$, MoO_2
1188	20	17.01	N/A	Passivates after 6 h	$MoSi_2$, Mo_5Si_3, SiO_2
1291	10	11.77	N/A	Passivates after 1.5 h	$MoSi_2$, Mo_5Si_3, SiO_2
1395	10	9.25	N/A	passivates after 0.5 h	$MoSi_2$, Mo_5Si_3, SiO_2
1498	4	6.52	N/A	Nonpassivating, nonlinear oxidation	$MoSi_2$, Mo_5Si_3

†Sample was rendered unsuable during sample preparation.

The samples exposed to 980 and 1084 K display rapid oxidation with two separate kinetic regions, the second much more rapid than the first. The 980 and 1084 K water vapor samples swelled and warped, as displayed in Fig. 3, during the exposure with mass gains after 20 h of 300 and 140 mg/cm^2, respectively.

The samples exposed to 670 and 773 K water vapor for 24 and 20 h, respectively, displayed less than 4 mg/cm^2 mass gain, equating to less that 1% overall mass change for each sample. Additionally, the 670 and 773 K samples display very little change upon visual inspection. The thermogravimetric (TG) results for 670–877 K exposures to both the air and water vapor samples are plotted in Fig. 4.

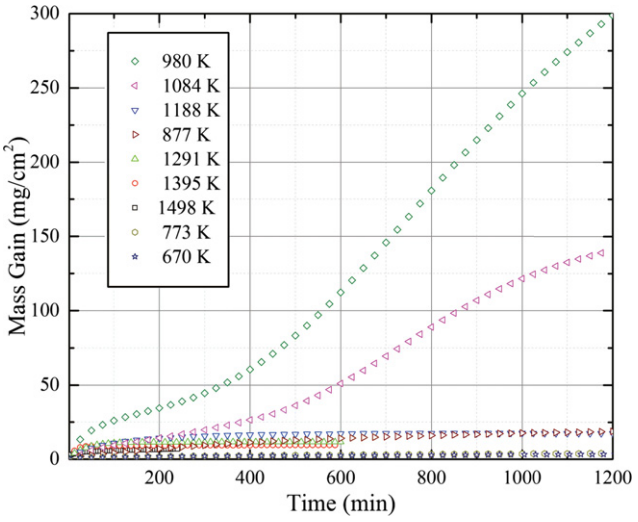

Fig. 2. Mass gain (mg/cm^2) vs time (min) data for $MoSi_2$ exposed to 670–1498 K isotherms in 0.55 ATM water vapor. The legend is ordered top to bottom by decreasing mass gain.

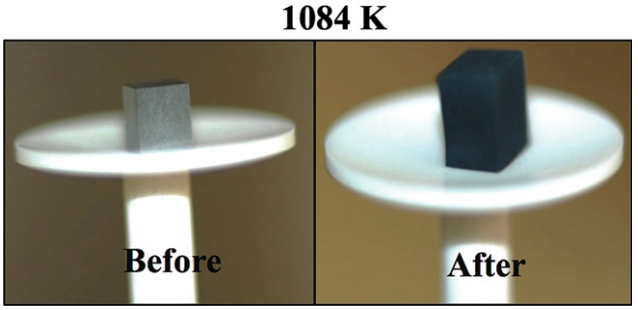

Fig. 3. Photographs of $MoSi_2$ before (left) and after (right) 1084 K steam exposure for 20 h.

Figure 5 compares the water vapor and air TG data for 1188–1498 K. $MoSi_2$ appears to passivate in both air and water vapor from 1188 to 1395 K, though the rate of mass

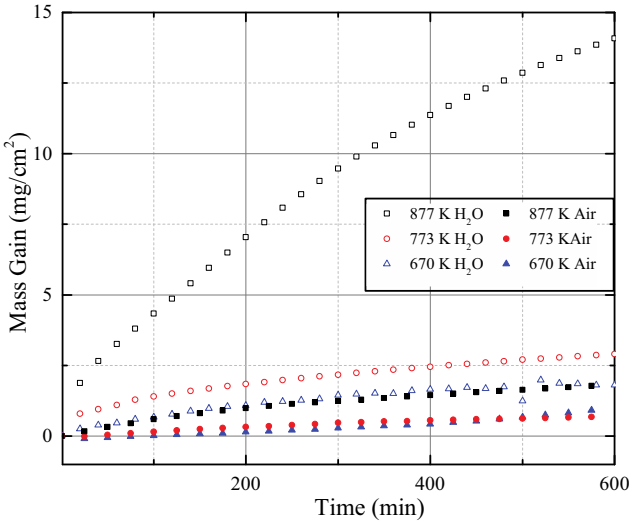

Fig. 4. Mass gain (mg/cm^2) vs time (min) data for $MoSi_2$ exposed to 670–877 K isotherms in 0.55 ATM water vapor (hollow symbols) and synthetic air (solid symbols). The legend is ordered top to bottom by decreasing mass gain.

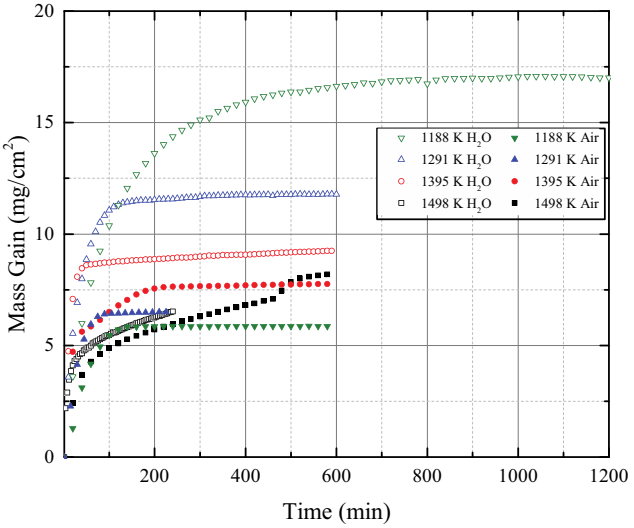

Fig. 5. Mass gain (mg/cm^2) vs time (min) data for $MoSi_2$ exposed to 1188–1498 K isotherms in 0.55 ATM water vapor (hollow symbols) and synthetic air (solid symbols). The legend is ordered top to bottom by decreasing mass gain in the water vapor samples.

gain decreases, indicating diffusion limited oxidation, much sooner in air than in water vapor. For both 1498 K samples, the oxidation rate decreases to a comparatively elevated linear mass gain, indicating that the samples are not passivating. These samples are further investigated using SEM.

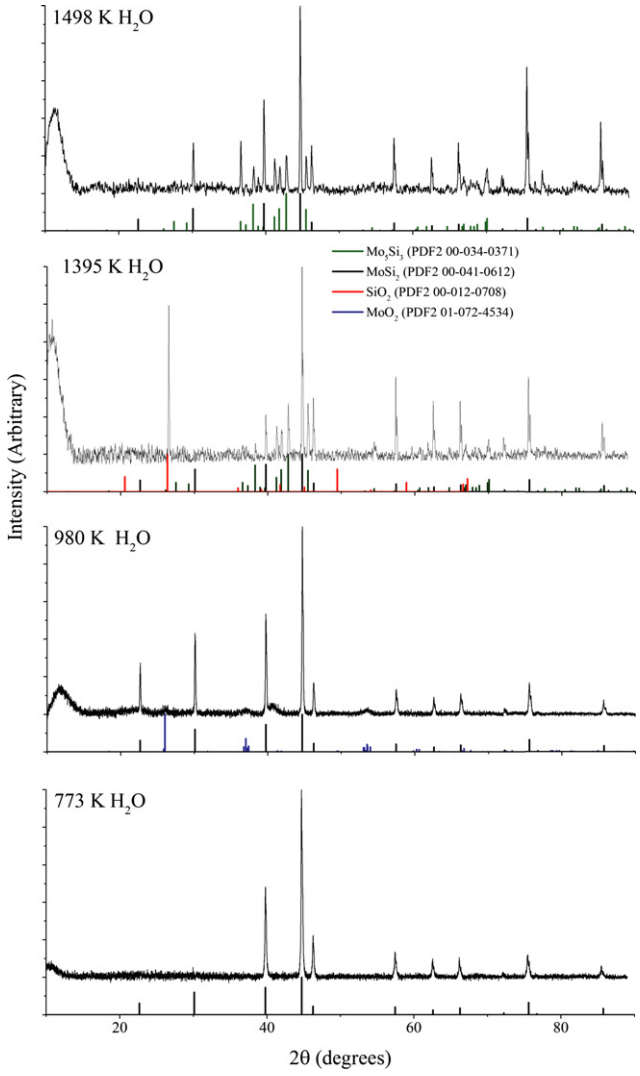

Fig. 6. Diffraction patterns for the 1498, 1395, 980, and 773 K sample surfaces following oxidation in water vapor.

(2) X-Ray Diffraction

X-Ray diffraction (XRD) patterns of the 773, 980, 1395, and 1498 K water vapor sample surfaces are displayed in Fig. 6. These four diffraction patterns help to summarize the varied effects of water vapor on $MoSi_2$ in the regions identified in the Discussion section of this paper. Diffraction patterns were also collected for the air samples, although those results are less informative since the oxide layer formed is much thinner than the interaction depth of the X-rays with the sample surface.

(3) Microscopy Results

Both surface and cross-sectional SEM were used to analyze the resulting microstructure of each sample. The most rapid oxidation is observed at 980 and 1084 K. Figure 7 displays the as-oxidized surface of a $MoSi_2$ sample after a 20 h, 1084 K water vapor exposure in increasing magnification from left to right. The 1084 K sample displays large oxide grains. In comparison, Fig. 8 displays the top-down perspective of a $MoSi_2$ sample after a 20 h, 1188 K water vapor exposure in increasing magnification from left to right. The 1188 K sample has formed a finer-grained oxide than the sample exposed to 1084 K water vapor. In addition, the layer is less cracked and uniformly covers the sample surface.

Micrographs of the cross-sections of the 670, 1084, and 1498 K water vapor samples are displayed in Figs. 9–11 to illustrate three of the four distinct behaviors observed in the water vapor TG data displayed in Section IV(1). The 670 K sample displayed in Fig. 9 exhibits a similar microstructure to the as-received material displayed in Fig. 12, with uniformly distributed pores. There is no observable oxide layer from the cross-sectional view of the sample. The 773 K sample displayed the same microstructure as the 670 K sample, with no visible oxide layer in the micrographs and the bulk of the material having similar structure to the as-received material.

The 1084 K sample displayed in Fig. 10, which exhibits dramatic mass gain in Fig. 2, appears to be completely reacted, with grain boundaries exposed throughout the sample. Likewise, the 980 K exposure resulted in the same full sample deterioration as the 1084 K sample shown in Fig. 10.

Finally, the 1498 K sample shown in Fig. 11 has formed a region of increased porosity approximately 80 μm in depth, expanding from the edge of the cross-section into the bulk of the sample. Both the air and the water vapor 1498 K samples exhibit similar trends of continued oxidation while the 1188–1395 K samples passivated in both atmospheres. Figure 13 compares the 1498 K synthetic air and water vapor exposed samples. It should be noted that the synthetic air sample experienced a 10 h isothermal hold while water vapor isotherm was only 4 h.

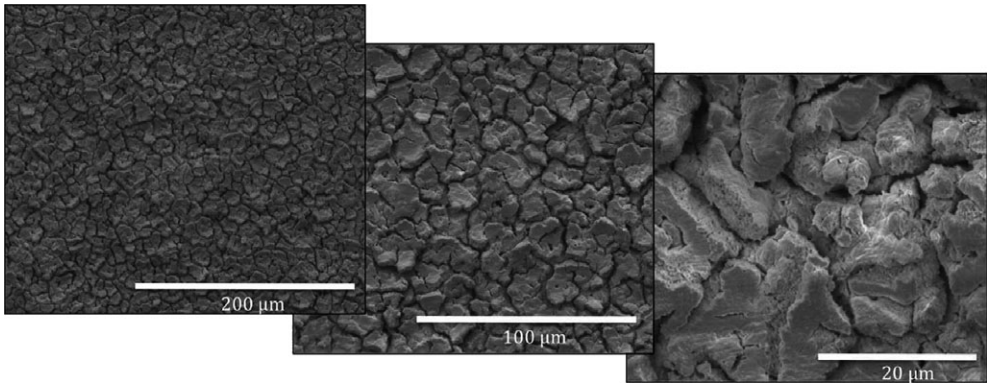

Fig. 7. Top-down SEM micrographs of $MoSi_2$ samples after a 20 h, 1084 K water vapor exposure.

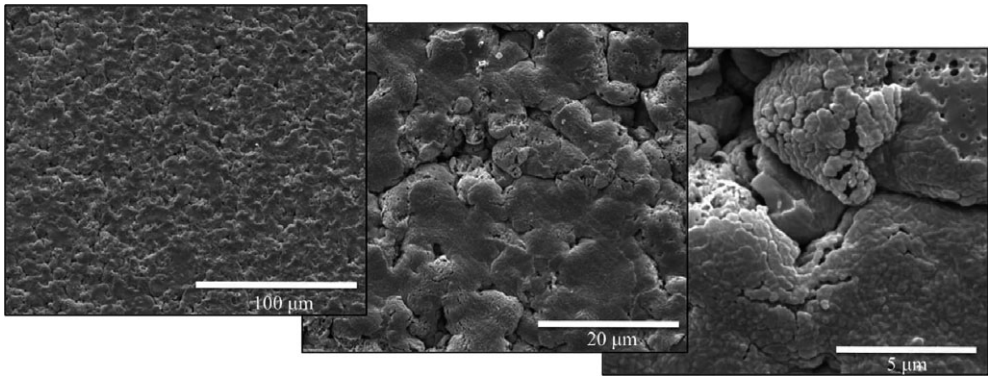

Fig. 8. Top-down SEM micrographs of $MoSi_2$ samples after a 20 h, 1188 K water vapor exposure.

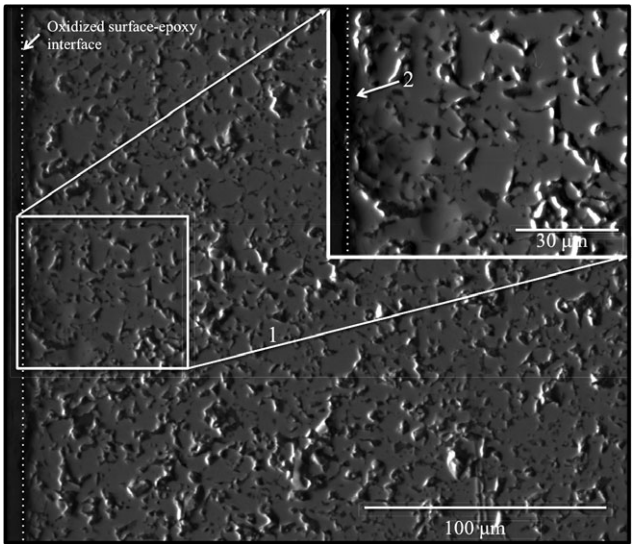

Fig. 9. Cross-sectional SEM micrographs of the $MoSi_2$ after 24 h, 670 K water vapor exposure.

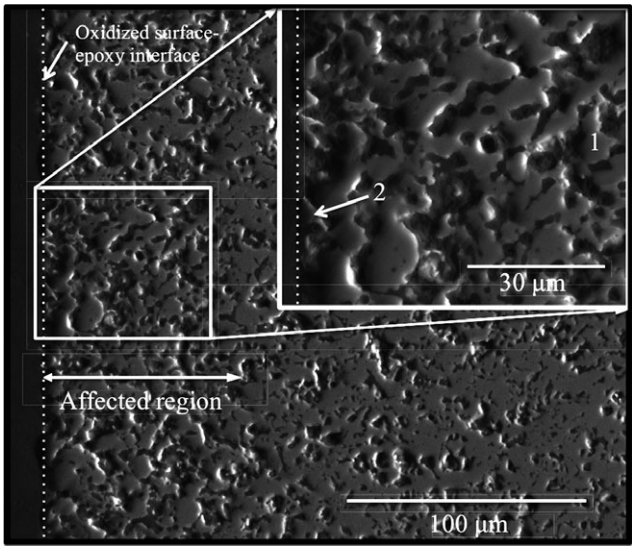

Fig. 11. Cross-sectional SEM micrographs of the $MoSi_2$ after 4 h, 1498 K water vapor exposure.

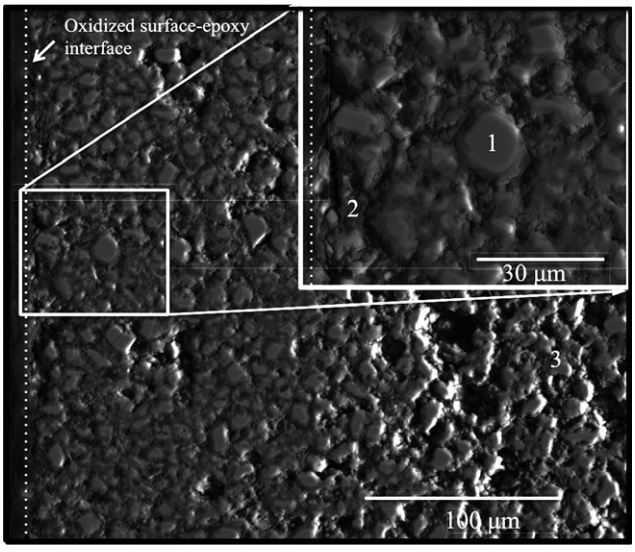

Fig. 10. Cross-sectional SEM micrographs of the $MoSi_2$ after 20 h, 1084 K water vapor exposure.

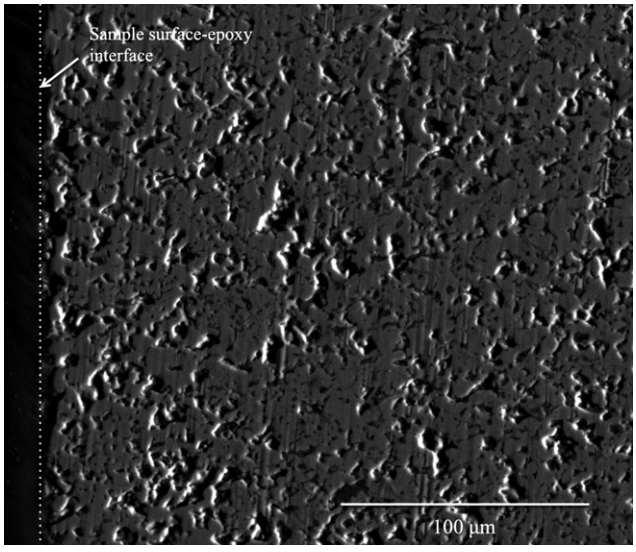

Fig. 12. Backscatter, cross-sectional SEM micrographs of the as-received $MoSi_2$.

The air sample displayed on the left of Fig. 13 shows uniform porosity, similar to the seemingly unaffected 670 K sample in Fig. 9.

(4) Elemental Analysis

Energy dispersive spectroscopy analysis was performed on several water vapor and air exposed samples to qualitatively assess the elemental composition of the various phases identified in BSED. Elemental standards were not used to calibrate

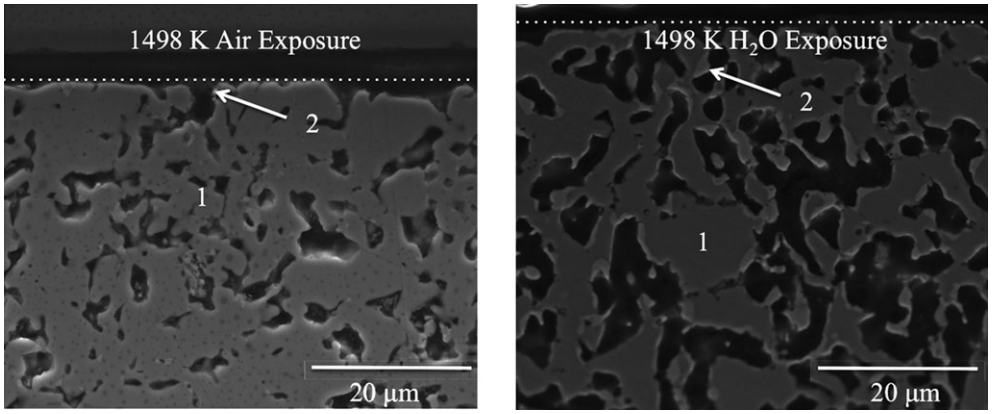

Fig. 13. Backscatter, cross-sectional SEM micrographs of $MoSi_2$ samples after 10 h, 1498 K synthetic air exposure (left) and 4 h, 1498 K water vapor exposure (right).

the detector prior to analysis, therefore the presented analysis is considered qualitative. In addition, EDS is not the ideal method to quantify small levels of oxygen in materials; it is used here to identify relative changes in the oxygen content and Mo/Si ratio across the samples' surfaces.

The spot analysis results for the regions identified in Figs. 9, 10, 11, and 13, are reported in Table II. Line scans of the cross-sectioned samples were performed, analyzing from the oxidation interface of each sample to 50 μm into the bulk of each sample. Due to the porosity of these samples, the data acquired displays a significant amount of fluctuation as the beam traverses pores in the material. However, the ratio of Mo/Si as compared to the as-received material provides insight to the compositional variation through the cross-section of the exposed samples. Figure 14 displays the line scans for the 670, 1084, and 1498 K water vapor exposures. The 1498 K water vapor exposure is also compared to the 1498 K air exposed sample.

Energy dispersive spectroscopy did not reveal any elevated oxygen levels in either the bulk or along the edges of the 670 and 773 K samples. There are elevated oxygen levels across the cross-sectioned sample of the 1084 K sample identified by EDS, indicating oxide formation deep into the bulk of the sample. EDS indicates that oxygen is only present on the very edge (top of the 1498 K air sample), in the lighter region of the material. Each pore in the 80 μm affected region of the water vapor sample exhibits a similar lighter outlining area which also contained oxygen, as seen in Fig. 13.

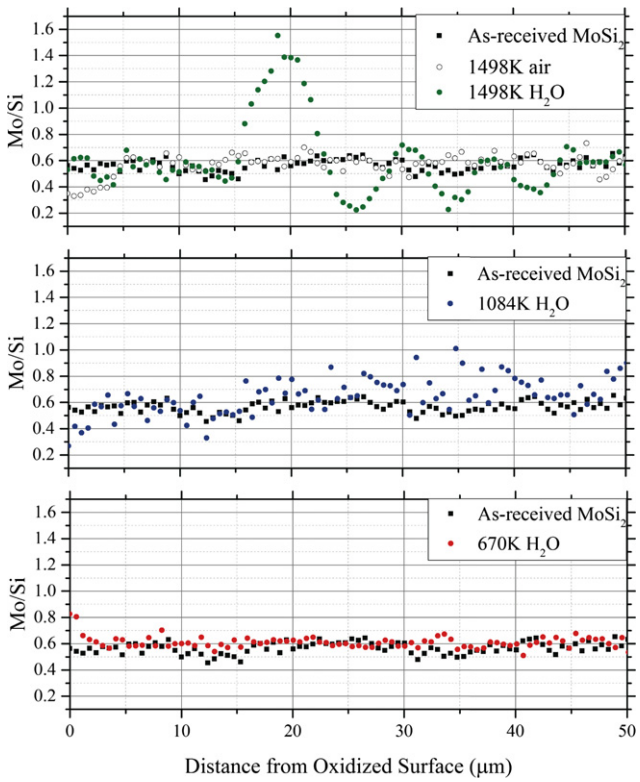

Fig. 14. Mo/Si ratio measured using EDS line scans from the oxidized surface to 50 μm into the cross-section sample for 670, 1084, and 1498 K as compared to the as-received material.

IV. Discussion

The material obtained from GoodFellow was measured to be 80% theoretical $MoSi_2$ density (6.26 g/cm^3). A cross-section micrograph of the as-received material is displayed in Fig. 12. The effects of porosity on the oxidation behavior of $MoSi_2$ was studied using 70% dense materials in a previous investigation by Kurokawa *et al.*[10] The authors noted a change in the oxidation kinetics and overall increase in mass gain of the porous $MoSi_2$ in 773 K air; however, the oxidation behavior observed in the present study agrees with accepted oxidation kinetics at both high and low temperature.[11] In addition, passivation of $MoSi_2$ is observed in air above 877 K, in agreement with past experiments, although at increased total oxidation. Therefore the authors believe

Table II. EDS Spot Analysis for Figs. 9–11

Sample		O K	Si K	Mo L
670 K H_2O	Fig. 9			
	Spot 1	4.23	65.45	30.32
	Spot 2	6.35	64.6	29.05
1084 K H_2O	Fig. 10			
	Spot 1	4.21	65.57	30.22
	Spot 2	18.26	56.10	25.64
	Spot 3	13.87	58.58	27.56
1498 K H_2O	Fig. 11			
	Spot 1	5.38	64.87	29.75
	Spot 2	30.06	39.08	30.86
1498 K H_2O	Fig. 12			
	Spot 1	—	64.87	29.75
	Spot 2	41.9	29.07	29.44
1498 K air	Fig. 12			
	Spot 1	—	66.25	33.75
	Spot 2	46.71	27.99	25.30

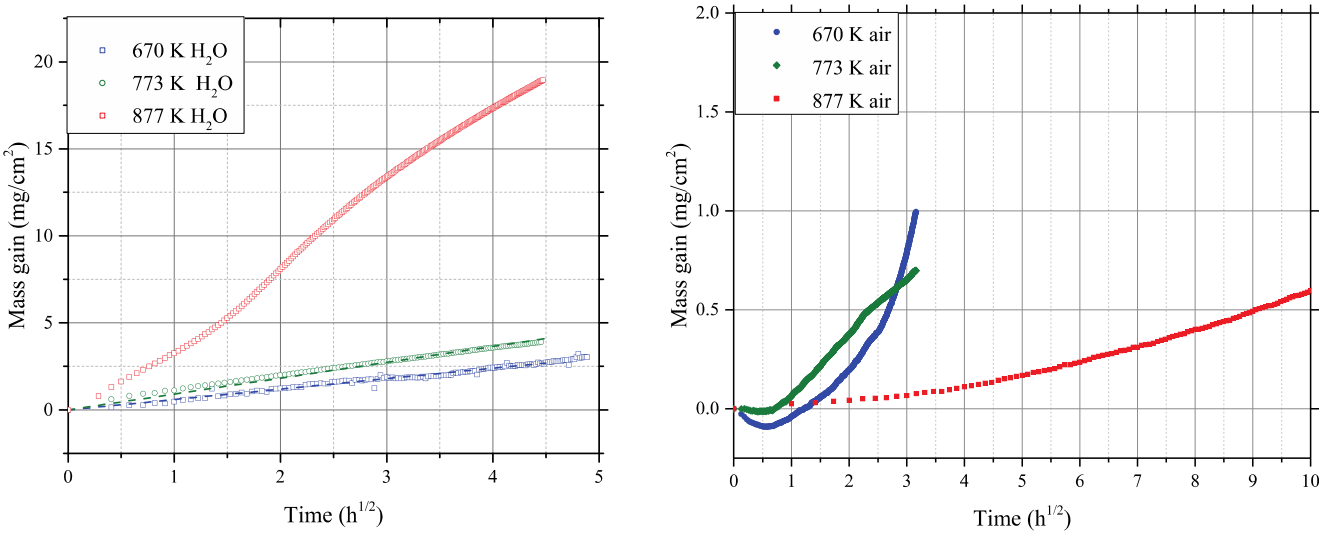

Fig. 15. 670–877 K water vapor (left) and air (right) TGA data plotted in mass gain (mg/cm^2) vs h$^{1/2}$. Note the different scales for both the mass gain and time axis in the two plots.

that the kinetic behavior and microstructural changes to this material are not affected by porosity, although the total oxidation of each sample measured by thermogravimetric analysis is expected to be higher in the 80% dense material than in a fully dense sample.

(1) 670–773 K Oxidation Behavior

The data for 670–877 K water vapor (left) and synthetic air (right) exposures is replotted in Fig. 15. The *x*-axis units are h$^{1/2}$, allowing for a clear view of the parabolic nature of the 670–773 K water vapor mass gain curves. Longer duration tests are necessary to determine if the resulting material is passivating in water vapor at these lower temperature exposures to water vapor, where in O_2 containing atmospheres the materials is known to "pest". The air curves do not display signs of parabolic oxidation, which is to be expected, given the documented pest formation in this temperature range. The oxidation rate in the water vapor of $MoSi_2$ is expected to decrease as a function of time, due to the diffusion limited, parabolic oxidation kinetics displayed at 670–773 K.[12,13]

It is expected that the volatile $MoO_2(OH)_2$, formed via the reaction displayed in Eq. (5), contributes to the change in oxidation dynamics seen at 670–773 K in water vapor. Though the thermodynamics are not favorable in this temperature range according to the data plotted in Fig. 1, The reaction has been stated in the literature to occur even at these lower temperatures.[14,15]

$$MoO_3 + H_2O(g) \rightarrow MoO_2(OH)_2(g) \quad (5)$$

In dry O_2 containing atmospheres, MoO_3 volatility aids in homogeneous SiO_2 scale formation with Mo_5Si_3 intermetallic formed between the native $MoSi_2$ and oxide scale via the reaction presented in Eq. (2), thus leading to passivation above 873 K.[6,8,5] Similarly, it is argued here, at 670–773 K, the $MoO_2(OH)_2$ volatility allows for a more passive oxide formation, primarily SiO_2. In a previous study, the hydroxide volatility was displayed as linear mass loss of Mo exposed to steam as low as 823 K where in air MoO_2 remained a stable oxide on the surface of the Mo sample.[7] In addition to SiO_2 formation, MoO_2 is also formed at this temperature range during steam oxidation. In high temperature steam, the ΔG of the reaction between H_2O and MoO_2 resulting in MoO_3 and H_2 is positive across this temperature range as is the reaction forming the hydroxide. Therefore, it is anticipated that MoO_2 will form via the reaction displayed in Eq. (6) and plotted in Fig. 1 but will remain on the surface unless the kinetics are sufficiently favorable to convert it into MoO_3 or $MoO_2(OH)_2$.

$$MoSi_2 + 6H_2O(g) \rightarrow MoO_2 + 2SiO_2 + 6H_2 \quad (6)$$

MoO_2 formation has been observed in Mo steam oxidation testing, and while it could provide a diffusion barrier to further oxidation in steam, it is rapidly oxidized to MoO_3.[16] At lower temperatures (below 1223 K), some MoO_2 remains on the surface. It is observed in the XRD data for the 980 K water vapor sample, though not enough MoO_2 was formed at 670–773 K to be detected via XRD.

(2) 877–1084 K Oxidation Behavior

At 877 K, the oxidation kinetics is no longer parabolic in water vapor, reference Fig. 15. In addition, the mass gain displayed after 20 h has increased by nearly a factor of five when compared to the 773 K water-vapor exposure. This supports the conclusion that the oxidation of $MoSi_2$ in water vapor is no longer diffusion limited. In this temperature regime, both MoO_3 and $MoO_2(OH)_2$ are volatile species.[17] The XRD data of the 980 K water-vapor sample displays $MoSi_2$ and broad MoO_2 peaks, where as only Mo_5Si_3 and SiO_2 phases were found in the air sample. This suggests that $MoSi_2$ oxidized in this temperature regime is incapable of forming a uniform SiO_2 required for passivation. Though there are signs (low angle, broad peak in XRD data) that some amorphous oxide could have formed.

The 980–1084 K samples were observed to swell and warp following testing, see Fig. 3. Oxidation penetrating throughout the bulk of $MoSi_2$ at 973–1073 K water vapor is attributed here to the lack of uniform SiO_2 formation in water vapor at these temperatures, likely due to the formation of MoO_2 observed in XRD analysis (reference Fig. 6) throughout the bulk of the reacted sample inhibiting the formation of a uniform SiO_2 layer.

(3) 1188–1395 K Oxidation Behavior

It is in the 1188–1395 K temperature range that the water vapor and air data display similar oxidation trends with two linear oxidation regions, the first more rapid than the second. Figure 5 shows the mass gain curves in both atmospheres to be very similar. The XRD data displays both Mo_5Si_3 and

SiO_2 in these water vapor samples, similar to the passivated air samples. However, MoO_2 is seen in some low intensity, broad peaks. The higher mass gain observed in the water vapor samples is likely caused by the continued formation of MoO_2. Likewise, while not displayed here, the SEM data showed very little porosity after the 1188 K water vapor exposure, and even less porosity in the 1291–1395 K samples. In this temperature regime, while there is an increase in mass gain, $MoSi_2$ passivates in water vapor.

(4) 1498 K Oxidation Behavior

While the TG data for the 1498 K air and water vapor exposures display similar oxidation trends, the effect of the water vapor exposure on the resulting microstructure is vastly different than the air exposure as exhibited in Fig. 13. The 1498 K water vapor sample displays increased porosity and oxygen rich regions outlining the pores. This indicates that $MoSi_2$ was not passivating at 1498 K in water vapor, where it formed only a small surface oxide layer in synthetic air. The behavior in water vapor is attributed here to a second volatile hydroxide. SiO_2 forms a volatile hydroxide $Si(OH)_4$ via the reaction described in Eq. (7).[18–20] Though the energetics of this reaction and the other volatile hydroxides known to form from SiO_2 reactions with steam were not available to the authors.

$$SiO_2 + 2H_2O(g) \rightarrow Si(OH)_4(g) \quad (7)$$

SiO_2 is identified via XRD in the water vapor samples exposed to temperatures exceeding 1084 K. SiO_2 has been found to exhibit porosity when exposed to T >1473 K water vapor.[18,21] It is expected that starting at temperatures greater than 1473 K $MoSi_2$ will not passivate during oxidation under water vapor environments. SiO_2 is not identified in the 1498 K sample surface, though Mo_5Si_3 is detected, as shown in Fig. 6. This further indicates that SiO_2 was likely formed via the reaction described in Eq. (2) but was volatilized at this temperature.

V. Conclusions

$MoSi_2$ displays different oxidation behavior in water vapor than in dry air. In the 670–1498 K temperature range, four distinct behaviors are observed. Parabolic oxidation is exhibited in only 670–773 K water vapor, a temperature range in which the material pests in dry O_2 environments. From 877–1084 K in water vapor, $MoSi_2$ undergoes rapid mass gain resulting in oxidation throughout the bulk of the sample at 980 and 1084 K. The resulting material displays swelling and warping after the 980–1084 K exposures. $MoSi_2$ exhibits the greatest resistance to water vapor oxidation in the 1188–1395 K temperature range, passivating and displaying very little visual or microstructural signs of oxidation. At 1498 K, the passivating SiO_2 layer is volatilized as a hydroxide in water vapor environments, degrading its performance.

The two volatile hydroxides $MoO_2(OH)_2(g)$ and $Si(OH)_4(g)$ play significant roles in the behavior of $MoSi_2$ in water vapor. The first facilitates uniform SiO_2 formation and leads to parabolic oxidation kinetics, slowing the oxidation reaction at 670–773 K. The second removes the protective SiO_2 layer, rendering the material susceptible to further oxidation at temperatures above 1473 K.

Acknowledgments

This work was supported by the U.S. Department of Energy, Office of Nuclear Energy Fuel Cycle Research and Development program. The authors thank Ming Tang for his help in imaging the 1498 K samples.

References

[1]O. Hnigschmid, "ber das Molybdnsilicid $MoSi_2$, das Wolframsilicid WSi_2 und das Tantalsilicid $TaSi2_2$," *Monatshefte fr Chemie und verwandte Teile anderer Wissenschaften*, **28** [8] 1017–28 (1907).

[2]Z. Yao, J. Stiglich, and T. Sudarshan, "Molybdenum Silicide Based Materials and Their Properties," *J. Mater. Eng. Performance*, **8** [3] 291–304 (1999).

[3]T. Chou and T. Nieh, "Pesting of the High-Temperature Intermetallic $MoSi_2$," *J. Miner. Metals Mater. Soc. (TMS)*, **45** [12] 15–21 (1993).

[4]K. Hansson, M. Halvarsson, J. Tang, R. Pompe, M. Sundberg, and J.-E. Svensson, "Oxidation Behaviour of a $MoSi_2$-Based Composite in Different Atmospheres in the Low Temperature Range (400–550°C)," *J. Eur. Ceram. Soc.*, **24** [13] 3559–73 (2004). Available at: http://www.sciencedirect.com/science/article/pii/S0955221903008975 [accessed on 19 October 2015].

[5]T. Chou and T. Nieh, "New Observations of $MoSi_2$ Pest at 500°C," *Scr. Metall. Mater.*, **26** [10] 1637–42 (1992). Available at: http://www.sciencedirect.com/science/article/pii/0956716X9290270O [accessed on 19 October 2015].

[6]C. Wirkus and D. Wilder, "High-Temperature Oxidation of Molybdenum Disilicide," *J. Am. Ceram. Soc.*, **49** [4] 173–7 (1966).

[7]A. Nelson, E. Sooby, Y.-J. Kim, B. Cheng, and S. Maloy, "High Temperature Oxidation of Molybdenum in Water Vapor Environments," *J. Nucl. Mater.*, **448** [13] 441–7 (2014). Available at: http://www.sciencedirect.com/science/article/pii/S0022311513011938 [accessed on 27 November 2015].

[8]T. Chou and T. Nieh, "Kinetics of $MoSi_2$ Pest During Low-temperature Oxidation," *J. Mater. Res.*, **8** [07] 1605–10 (1993).

[9]K. Hansson, J. Tang, M. Halvarsson, R. Pompe, M. Sundberg, and J.-E. Svensson, "The Beneficial Effect of Water Vapour on the Oxidation at 600 and 700°C of a $MoSi_2$-Based Composite," *J. Eur. Ceram. Soc.*, **25** [1] 1–11 (2005). Available at: http://www.sciencedirect.com/science/article/pii/S0955221904000299 [accessed on 19 October 2015].

[10]K. Kurokawa, H. Houzumi, I. Saeki, and H. Takahashi, "Low Temperature Oxidation of Fully Dense and Porous $MoSi_2$," *Mater. Sci. Eng.: A*, **261** [1] 292–9 (1999).

[11]Y. Liu, G. Shao, and P. Tsakiropoulos, "On the Oxidation Behaviour of $MoSi_2$," *Intermetallics*, **9** [2] 125–36 (2001).

[12]C. Wagner, "Theoretical Analysis of the Diffusion Processes Determining the Oxidation Rate of Alloys," *J. Electrochem. Soc.*, **99** [10] 369–80 (1952).

[13]N. Cabrera and N. Mott, "Theory of the Oxidation of Metals," *Rep. Prog. Phys.*, **12** [1] 163–84 (1949).

[14]G. Belton and A. Jordan, "The Volatilization of Molybdenum in the Presence of Water Vapor," *J. Phys. Chem.*, **69** [6] 2065–71 (1965).

[15]T. Millner and J. Neugebauer, "Volatility of the Oxides of Tungsten and Molybdenum in the Presence of Water Vapour," *Nature*, **163**, 601–2 (1949).

[16]M. Kilpatrick and S. K. Lott, "Reaction of Flowing Steam with Refractory Metals. 1, 2 i. Molybdenum (1100–1700)," *J. Phys. Chem.*, **69** [5] 1638–40 (1965).

[17]P. E. Blackburn, M. Hoch, and H. L. Johnston, "The Vaporization of Molybdenum and Tungsten Oxides," *J. Phys. Chem.*, **62** [7] 769–73 (1958).

[18]T. Cheng and P. F. Tortorelli, "Silicon Carbide 389 Oxidation in High-Pressure Steam," *J. Am. Ceram. Soc.*, **96** [7] 2330–7 (2013).

[19]E. J. Opila, N. S. Jacobson, D. L. Myers, and E. H. Copland, "Predicting Oxide Stability in High-Temperature Water Vapor," *J. Miner., Metals Mater. Soc. (TMS)*, **58** [1] 22–28 (2006).

[20]E. J. Opila, D. S. Fox, and N. S. Jacobson, "Mass Spectrometric Identification of Si-O-H(g) Species from the Reaction of Silica with Water Vapor at Atmospheric Pressure," *J. Am. Ceram. Soc.*, **80** [4] 1009–12 (1997).

[21]K. A. Terrani, B. A. Pint, C. M. Parish, C. M. Silva, L. L. Snead, and Y. Katoh, "Silicon Carbide Oxidation in Steam up to 2MPa," *J. Am. Ceram. Soc.*, **97** [8] 2331–52 (2014). □